Climate Dynamics (2023) 61:3327–3341
https://doi.org/10.1007/s00382-023-06733-7

The compound impacts of sea surface temperature modes in the Indian and North Atlantic oceans on the extreme precipitation days in the Yangtze River Basin

Zhiwei Zhu[1] · Yongning Feng[1] · Wei Jiang[2] · Rui Lu[1] · Ying Yang[1]

Received: 14 November 2022 / Accepted: 22 February 2023 / Published online: 14 March 2023

Abstract

Owing to the East Asian summer monsoon, extreme precipitation occurred frequently over the Yangtze River Basin (YRB), leading to flooding and secondary disasters. Therefore, understanding the physical mechanism and seeking predictability sources of extreme precipitation in the YRB are of scientific and practical importance. The present study examines the independent and compound impacts of leading sea surface temperature (SST) modes in the Indian Ocean and the North Atlantic Ocean on summer extreme precipitation days (EPDs) over the YRB.

The Indian Ocean basin-wide uniform SST mode (the Indian Ocean Basin Mode) influences the EPDs over the YRB by inducing a Kelvin wave response and the Pacific–Japan pattern, whereas the two leading SST modes of the North Atlantic Ocean show different meridional tripole patterns with different climate impacts on East Asia. The North Atlantic SST tripole southern mode (NATS) induces quasi-stationary Rossby wave trains over mid-latitude Eurasia and the tropical waves that influence the EPDs in the YRB. The North Atlantic SST tripole northern mode (NATN) impacts the circulation anomaly over Northeast Asia through inducing different Eurasian quasi-stationary Rossby wave trains.

When the IOBM and the NATS are both in the positive phase, enhanced EPDs occur over the YRB. On the one hand, the IOBM induces a Kelvin wave response, which strengthens the western North Pacific anomalous anticyclone (WNPAC). On the other hand, the NATS stimulates the mid-latitude quasi-stationary Rossby waves and results in the Northeast Asia anomalous cyclone (NEAC). The warm, moist air over the northwestern flank of the WNPAC and the cold, dry air over the southern flank of the NEAC converge in the YRB, leading to more EPDs in the region. When the IOBM and the NATN are out of phase, the Kelvin wave response in terms of the WNPAC induced by the IOBM warming is modulated by the negative phase of the NATN via quasi-stationary Rossby wave trains over mid-latitude Eurasia, resulting in more EPDs in the YRB.

Based on the compound effect of different SST modes in the two ocean basins, the year-to-year EPDs over the YRB can be reconstructed reasonably well, which provides useful predictability sources for the seasonal prediction.

Keywords Summer extreme precipitation days · Yangtze River Basin · Indian Ocean · North Atlantic Ocean · Mid-latitude rossby wave trains

1 Introduction

The Yangtze River Basin (YRB) is influenced by the prevailing East Asian summer monsoon, and therefore is prone to extreme precipitation, which leads to flooding and secondary disasters, threatening the safety of lives and property. For example, the severe floods in summer 1998 (Huang 2006), the heavy rainfall in summer 2016 (Sun et al. 2021) and the persistent extreme precipitation in summer 2020 (Liu and Ding 2020; Qiao et al. 2021) caused serious

✉ Zhiwei Zhu
zwz@nuist.edu.cn

[1] Key Laboratory of Meteorological Disaster, Collaborative Innovation Center on Forecast and Evaluation of Meteorological Disasters (CIC-FEMD), Joint International Research Laboratory of Climate and Environment Change (ILCEC), Ministry of Education (KLME), Nanjing University of Information Science and Technology, Ningliu Road 219, Nanjing 210044, China

[2] Jiangsu Climate Center, Nanjing 210041, China

casualties and property damage. Therefore, exploring the dynamic origins of summer extreme precipitation over the YRB is of scientific and social importance.

The favorable condition for precipitation in the YRB is the convergence of a warm, moist air mass and a cold, dry air mass (Li and Lu 2017), which is associated with different large-scale atmospheric circulation systems (Hu et al. 2019). These circulation systems include the western North Pacific anomalous anticyclone (WNPAC) (Chou et al. 2009; Wang et al. 2003; Zhang et al. 2017a; Liu et al. 2019), the Eurasian mid-to-high latitudes blocking high (Chen and Zhai 2014; He et al. 1995; Ding et al. 2021), the South Asia high (SAH) (Ren et al. 2015), and Northeast cold vortex (He et al. 2007; Xu and Qi 2022). WNPAC has a vital role in transporting a warm, moist air mass into the YRB, while the blocking high over the mid-latitude Eurasian continent and the enhanced SAH over the Tibetan Plateau lead to southward invasion of a cold, dry air mass (Zhang et al. 2021), favoring more precipitation in the YRB (Ning et al. 2017). Furthermore, the Northeast Cold Vortex also modulates the location and intensity of East Asian summer rainfall (Lu et al. 2021; Yang et al. 2023). In general, summer precipitation in the YRB is always a result of the combination of different critical anomalous circulation systems from both the tropics and the extra-tropics (Yuan et al. 2012; Li and Lu 2017; Liu et al. 2020).

Owing to the recurrent and persistent nature of sea surface temperature (SST) modes, the typical SST modes of different oceans are often used as physical predictors of long-term mean precipitation (Chung et al. 2011; Li et al. 2017; Liu et al. 2021). The diverse evolutions of the central-eastern tropical Pacific SSTA during the developing or decaying phase of El Niño-Southern Oscillation (ENSO) could modulate East Asia summer rainfall through wind-evaporation-sea surface temperature feedback (Wang et al. 2000, 2013; Chen et al. 2016; Li et al. 2017; Zhang et al. 2017b; Pan et al. 2021).

During the decay phase of ENSO episodes, the Indian Ocean Basin Mode (IOBM) exerts a delayed effect of ENSO on East Asia precipitation (Klein et al. 1999). The IOBM causes the WNPAC through a Kelvin wave response that propagates eastward to the western tropical Pacific (Yang et al. 2007; Wu et al. 2010; Xie et al. 2016; Chen et al. 2018; Cai et al. 2021; Tang et al. 2021). The IOBM warming also affects the ascending motion over subtropical Asia by shifting the East Asia westerly jet southward (Qu and Huang 2012), favoring more precipitation over the YRB (Zhou et al. 2021). Furthermore, the impact of the IOBM on the East Asian summer precipitation has become more remarkable because its warming center has shifted towards the Arabian Sea since the late 1970s (Sun et al. 2019). Another dominant SST mode over the Indian Ocean, the Indian Ocean Dipole (IOD) during autumn, is also closely connected with the Asian climate (Li and Mu 2001; Luo et al. 2010). As the IOD can transfer into the IOBM in the following summer (Takaya et al. 2020; Zhang et al. 2022), it has a significant correlation with the IOBM.

The Atlantic Ocean SST also notably influences the summer precipitation in the YRB. The sea surface temperature anomaly (SSTA) over the tropical North Atlantic stimulates convection in situ, inducing Gill-type responses (Gill 1980) in terms of tropical Kelvin and Rossby waves. While the tropical Kelvin wave propagates eastward and directly influences the precipitation in YBR through the WNPAC via a tropical route (Rong et al. 2010; Chen et al. 2015), the tropical Rossby wave response impacts the precipitation in the YRB from both tropical and extratropical routes. On the one hand, the northeasterly wind over the northwestern flank of the Rossby wave response in terms of lower level cyclonic anomaly suppresses the convection in central Pacific, which further influences the precipitation in the YRB by modulating the WNPAC (Ham et al. 2013; Hong et al. 2014; Jin and Huo 2018). On the other hand, the Rossby wave response in terms of upper level anticyclonic anomaly perturbs the westerly jet, which induces Eurasian mid-latitude Rossby wave trains and affects the East Asian circulation, influencing the precipitation in the YRB (Lu and Dong 2005; Yang et al. 2023; Lu et al. 2023). Besides, the meridional tripole SST pattern (Wu et al. 2012; Zuo et al. 2013; Li and Ruan 2018; Li et al. 2023) and the zonal dipole SST pattern (Yang et al. 2023) over the North Atlantic are also associated with the YRB precipitation anomalies via inducing Eurasian mid-latitude Rossby wave trains.

Previous studies mainly focused on the effect of the SST in a single ocean basin on summer precipitation in the YRB, and little attention has been paid to the compound impacts of different basins on the precipitation in the YRB, especially for the extreme precipitation in the region. Therefore, in this study, we investigate the compound impacts of the Indian Ocean and the North Atlantic Ocean SST modes on the summer extreme precipitation days (EPDs) in the YRB. The remainder of this paper is organized as follows. Section 2 introduces the datasets, methods and model used in this study. In Sect. 3, the leading modes of the SSTAs over the Indian Ocean and the North Atlantic Ocean and their linkages with summer EPDs in the YRB are investigated. Section 4 explores the compound impacts of the Indian Ocean and the North Atlantic Ocean SST modes on the summer EPDs in the YRB. Section 5 verifies the physical processes of the compound effect using numerical experiments. Discussion and conclusion are given in the last section.

2 Data, methods and model

2.1 Data

The datasets used include: (1) the daily gridded rainfall dataset derived from 2416 meteorological station records (CN05.1) with a horizontal resolution of 0.25° × 0.25° (Wu and Gao 2013); (2) the global monthly mean precipitation from the Global Precipitation Climatology Project Monthly Precipitation Climate Data Record with a horizontal resolution of 2.5° × 2.5° (Adler et al. 2018); (3) the monthly mean geopotential height, and zonal and meridional wind from the fifth-generation reanalysis of European Centre for Medium-Range Weather Forecasts with a horizontal resolution of 0.25° × 0.25° (Hersbach et al. 2020); (4) the monthly mean SST from the National Oceanic and Atmospheric Administration Extended Reconstructed SST dataset, version 5 with a horizontal resolution of 2.0° × 2.0° (Huang et al. 2017); (5) the monthly mean SST from the Met Office Hadley Centre Sea Ice and SST dataset with a horizontal resolution of 1.0° × 1.0° (Rayner et al. 2003). To eliminate uncertainty from the different dataset, the two SST datasets are averaged. All datasets cover the time span from 1979 to 2020. In this study, summer denotes the seasonal mean from June to August (JJA).

2.2 Methods

As the precipitation shows remarkable regional differences over China, EPDs are defined based on the percentile method (Moberg et al. 2006). The 90th percentile of the daily precipitation (larger than 0.1 mm per day) is chosen as the threshold of extreme daily precipitation for each grid point. If the daily rainfall is equal to or greater than the corresponding threshold, it is recorded as an EPD.

The dominant SST modes over the North Atlantic Ocean (0°–70°N, 90°W–15°E) and the Indian Ocean (30°S–30°N, 30°E–115°E) are extracted using empirical orthogonal function (EOF) analysis (Lorenz 1956). To exclude the impact of global warming, the SST was detrended before EOF analysis. To explore the associated meteorological fields with respect to different SST modes, linear regression analysis and composite analysis are used. Student's *t*-test is applied to assess their statistical significance. To understand the atmospheric teleconnections associated with different SST modes, the wave activity flux (WAF) is calculated based on the following formula proposed by Takaya and Nakamura (2001).

$$W = \frac{1}{2\left|\bar{U}\right|}\begin{bmatrix} \bar{u}\left(\psi_x'^2 - \psi'\psi_{xx}\right) + \bar{v}\left(\psi_x'\psi_y' - \psi'\psi_{xy}\right) \\ \bar{u}\left(\psi_x'\psi_y' - \psi'\psi_{xy}'\right) + \bar{v}\left(\psi_y'^2 - \psi'\psi_{yy}'\right) \end{bmatrix}$$

,where an overbar and a prime represent the climatological mean and anomaly, respectively; ψ and $U = (u, v)$ represent the streamfunction and the horizontal wind, respectively; and W denotes the two-dimensional Rossby WAF.

2.3 Model

The Community Atmosphere Model (CAM) version 5.3 is used to investigate the climate impacts of different SST modes. The CAM v5.3 is the atmosphere component of the Community Earth System Model (CESM), developed by the National Center for Atmospheric Research (Neale et al. 2010). CAM v5.3 has a T42 Gaussian grid horizontal resolution, and a σ–p hybrid vertical coordinate of 30 levels, with the top level at 3.643-hPa. Each experiment was integrated for 20 years, and the JJA mean of the outputs over the last 15 years are analyzed as the atmospheric response to the SST forcing. The design of the numerical experiments is described in detail in Sect. 5.

3 Leading SST modes and their linkage to EPDs in the YRB

3.1 Dominant SST modes over Indian and North Atlantic oceans

To investigate the leading SST modes over the Indian Ocean and the North Atlantic Ocean, EOF analysis was conducted using the summer mean (JJA) SST over the two ocean basins during 1979–2020. Figure 1a shows the spatial pattern of the first mode of the Indian Ocean SST, which accounts for 35.8% of the total variance. The spatial pattern of this leading mode is characterized by a basin-wide uniform pattern (the IOBM) with maximum positive loadings over the Arabian Sea and to the north and east of Madagascar. The principal component (PC) shows pronounced interannual and interdecadal variabilities (Fig. 1b). The first EOF mode is significant and well separated from the higher modes (Fig. 1c) (North et al. 1982).

Figure 1d, f shows the spatial pattern of first two EOF modes of the North Atlantic SST, which accounts for 25.8% and 16.4% of the total variance, respectively. The first mode of North Atlantic SST (Fig. 1d) shows a meridional tripole structure, with positive loadings in tropical and subpolar Atlantic, and negative loadings in between. PC1 shows significant interannual and interdecadal variability (Fig. 1e). The second mode of North Atlantic SST (Fig. 1f) also shows a meridional tripole structure, but with positive loadings in the subpolar and subtropics and negative loadings in between. The corresponding PC2 shows significant interannual variability (Fig. 1g). These two modes are statistically

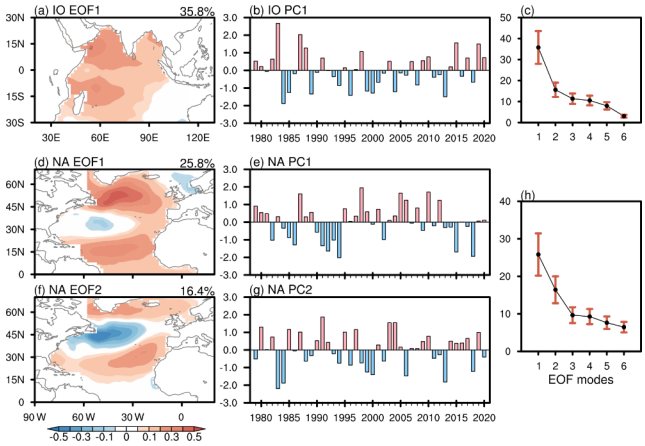

Fig. 1 The **a** spatial pattern and **b** normalized PC of the first EOF mode of summer SST over the Indian Ocean during 1979–2020. **c** The explained variances (black dots) of the first six modes of the Indian Ocean SST and their standard deviation of the sampling error (orange bars). **d**–**g** The same as in **a**–**b**, but for the first two EOF modes of summer SST over North Atlantic Ocean. **h** The same as in **c**, but for the Atlantic Ocean SST

significant and independent of each other, and they are also separated from higher modes. It is noted that although the first two leading SST modes both show tripole structures, their locations are quite different. The southern pole of the first tripole mode is located around 15°N, whereas the southern pole of the second tripole mode is mainly confined to the region between 15°N and 30°N. Given the different tripole locations of the two leading EOF modes, the first SST mode is defined as the North Atlantic tripole southern mode (NATS) and the second mode is defined as the North Atlantic tripole northern mode (NATN). In the following subsections, we explore the physical mechanism of these major SST modes (IOBM, NATS and NATN) on the summer EPDs in the YRB.

3.2 The anomalies associated with the IOBM

To explore the influence of the IOBM on the summer EPDs in the YRB, the dynamic and thermodynamic fields are regressed onto the PC of the first EOF mode of the Indian Ocean SST (Fig. 2). As shown in Fig. 2a–c, the Pacific–Japan (PJ) pattern (Nitta 1987), with an anomalous anticyclone over the western North Pacific (WNPAC) and an anomalous cyclone over Northeast Asia (NEAC), is associated with the Indian Ocean basin-wide warming. While the anomalous southwesterly wind on the northwestern flank of WNPAC enhances the transport of warm, moist air toward the YRB, the anomalous northwesterly wind on the southwestern flank of NEAC delivers a cold air mass to the YRB. The convergence of cold air and warm, moist air results in

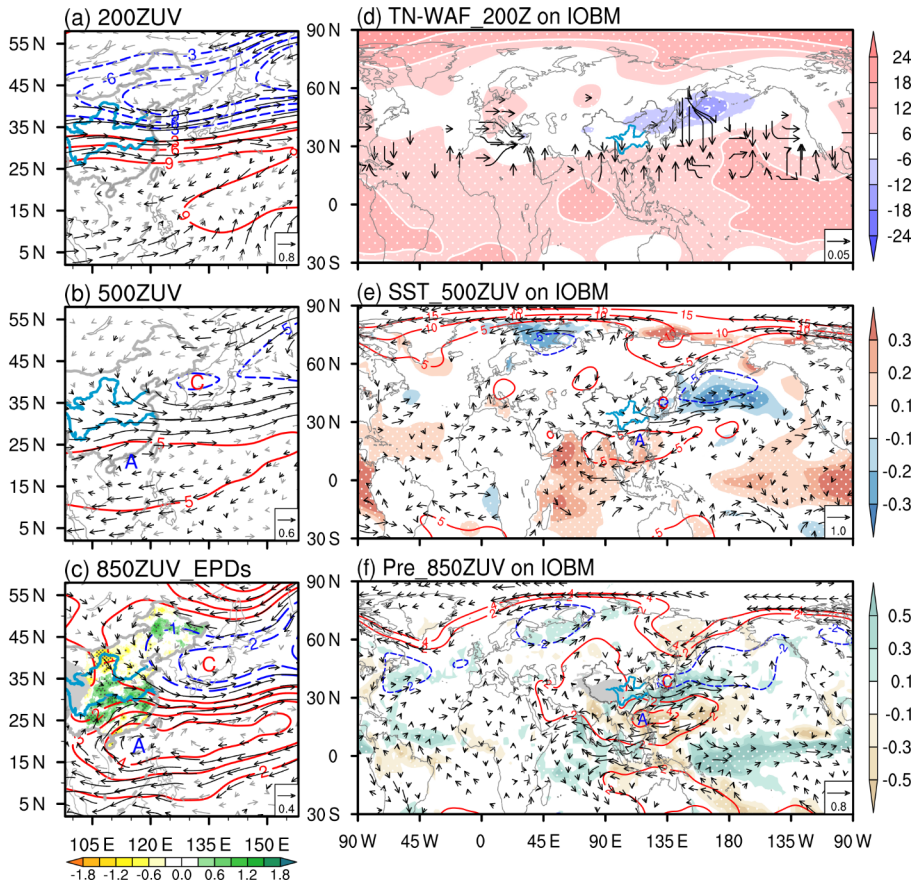

Fig. 2 The regressed summer mean **a** 200 hPa, **b** 500 hPa, and **c** 850 hPa geopotential height (contours; unit: gpm), wind (vectors; unit: m s^{-1}) over East Asia onto the Indian Ocean PC1, and **c** the associated EPDs (shading; units: day) over eastern China. The regressed summer mean **d** global 200 hPa geopotential height (contours; unit: gpm) and the associated WAF (vectors; unit: m^2 s^{-2}), **e** global 500 hPa geopotential height (contours; unit: gpm), wind (vectors; unit: m s^{-1}) and SST (shading; unit: °C), and **f** global 850 hPa geopotential height (contours; unit: gpm), wind (vectors; unit: m s^{-1}) and precipitation (shading; unit: mm d^{-1}) onto the Indian Ocean PC1. The letters A and C indicate the centers of anticyclonic and cyclonic anomalies, respectively. The regression coefficient of wind at the 90% confidence level is shown with black arrows; otherwise, shown with grey arrows. The shading with dots is significant at the 90% confidence level

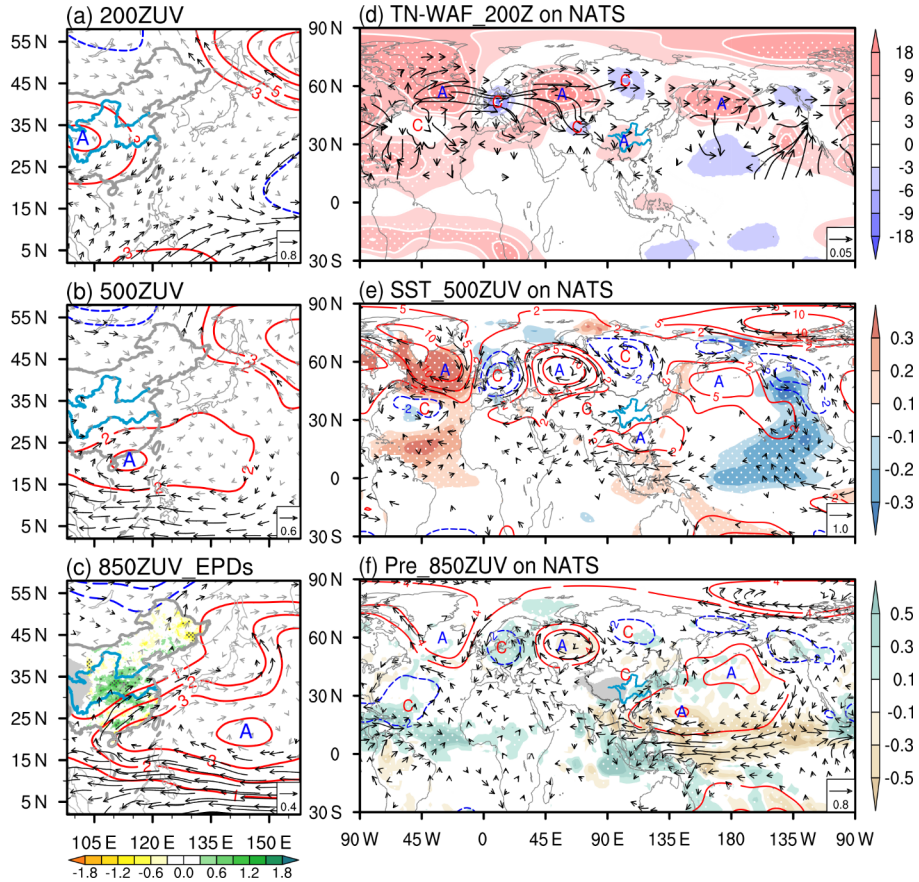

Fig. 3 The same as in Fig. 2, but for regression onto the PC1 of the North Atlantic SST

enhanced mean precipitation and positive EPD anomalies in the YRB.

The upper-level WAF shows inconspicuous upstream signals from Eurasia toward the YRB. However, the WAF emanating from the tropical Indo-Pacific region to East Asia is observed (Fig. 2d), suggesting that the origin of the PJ pattern may come from the tropical forcing. The warm SSTAs over the Indian Ocean result in local positive precipitation anomalies (Fig. 2e and f). The precipitation-induced diabatic heating stimulates the tropical Kelvin wave response from Indian Ocean to the western Pacific. The easterly Kelvin wave declines poleward, which further enhances the WNPAC (Xie et al. 2009; Wu et al. 2010). The WAF propagates northward, forming the PJ pattern. In sum, the IOBM warming results in positive EPD anomalies over the YRB during boreal summer by inducing the PJ pattern.

3.3 The anomalies associated with the NATS

To reveal the impact of the NATS on summer EPDs in the YRB, the local and global dynamic and thermodynamic fields are regressed onto PC1 of the North Atlantic SST (Fig. 3). In the context of the NATS mode, positive EPD anomalies occur over the central and north YRB (Fig. 3c). The enhanced EPDs are associated with the anomalous southwesterly wind on the northwestern flank of the low-level WNPAC. The anomalous southwesterly wind transports moisture into higher latitudes (Fig. 3c). Meanwhile, the upper-level anomalous anticyclone over the Tibetan Plateau also favors positive EPDs anomalies over central China via a pumping effect (Fig. 3a).

It is noted that although the upper-level and lower-level anomalous anticyclones are both closely related to the NATS, the influencing routes of the NATS are different. As shown in Fig. 3d, the upper-level anomalous anticyclone is associated with quasi-stationary Rossby wave trains over the mid-latitude Eurasian continent. The 200 hPa WAF emanates from the North Atlantic and propagates eastward, then divides into two branches over the Ural Mountains. While the northern branch goes northeastward to the eastern Siberia, the southern branch propagates southeastward to the Tibetan Plateau. The upper-level anomalous anticyclone of the southern branch of the Rossby wave train favors upper-level divergence, leading to the positive EPD anomalies via a pumping effect.

As shown in Fig. 3e and f, the middle-level and lower-level anomalous WNPAC is accompanied by enhanced convection over the tropical Atlantic Ocean and suppressed convection over the central/eastern tropical Pacific. On the one hand, the positive SSTA over the tropical Atlantic

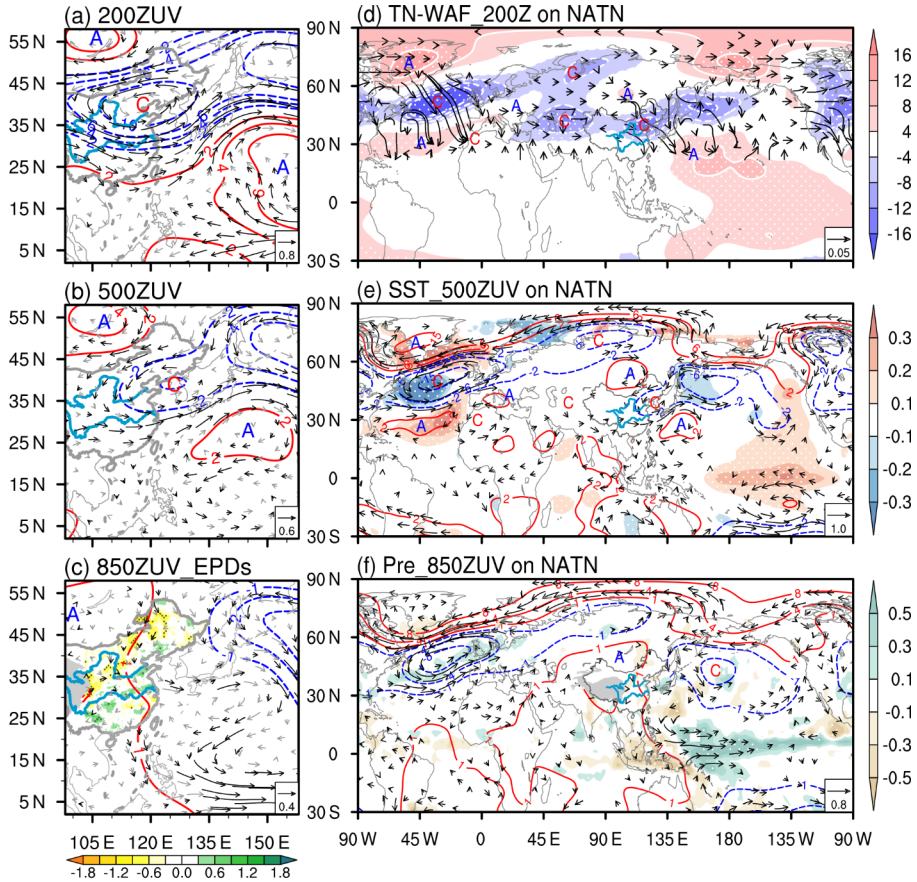

Fig. 4 The same as in Fig. 2, but for regression onto the PC2 of the North Atlantic SST

induces local positive precipitation anomalies, leading to a Gill-type Rossby wave response (Gill 1980) in terms of the lower-level cyclonic anomaly over the equatorial eastern Pacific. The northerly wind on the west of the cyclonic anomalies over the eastern Pacific superimposes on the northeast trade wind. Enhanced northeast wind as well as cold advection result in a negative SSTA (Fig. 3e) and suppressed convection (Fig. 3f) over the tropical east-central Pacific (Ham et al. 2013). The cold SSTA along with the suppressed convection induces a Rossby wave response in terms of the anticyclone anomalies, leading to the formation of the WNPAC. On the other hand, the enhanced convection over the tropical Atlantic stimulates a Kelvin wave response easterly wind across the Indo-Pacific region, which declines poleward, leading to the formation of WNPAC (Gill 1980). The northwestern flank of the lower-level WNPAC leads to positive EPD anomalies via the water vapor transport.

3.4 The anomalies associated with the NATN

To investigate the possible climate impact of the NATN on EPDs in the YRB, the local and global dynamic and thermodynamic fields are regressed onto PC2 of the North Atlantic SST (NATN). In Fig. 4a–c, it can be seen that in association with the positive phase of the NATN mode, the lower-level northerly anomalies control almost the whole eastern China, leading to negative EPD anomalies over northeastern China. At the upper level, a cyclonic anomaly dominates Northeast Asia, leading to upper convergence which is unfavorable for EPDs in the region. The WAF at 200 hPa (Fig. 4d) indicates that a quasi-stationary Rossby wave train emanates from the North Atlantic to mid-to-high-latitude Eurasia. The quasi-stationary Rossby wave train is characterized by four pairs of anomalous anticyclones/cyclones centered over the Greenland/northern North Atlantic, subtropical North Atlantic/North Africa, Mediterranean/Iran Plateau, and Lake Baikal/Northeast Asia, respectively. The cyclonic anomaly over Northeast Asia results in a general negative EPD anomaly over eastern China, with little influence on EPDs in the YRB.

4 Compound effect of SST modes of Indian Ocean and North Atlantic Ocean

The above analysis examined the individual impact of the IOBM, NATS and NATN modes on the summer EPDs in the YRB, respectively. As the PC of the Indian Ocean SST mode is independent of that of the NATS (NATN) mode with insignificant correlation coefficients of 0.16 (0.25), and

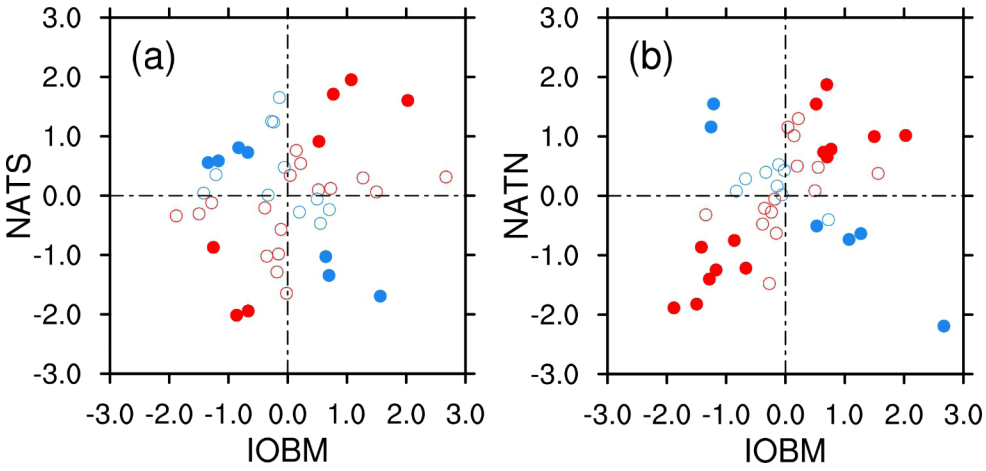

Fig. 5 **a** Scatter-plots based on normalized PCs of the IOBM and NATS. **b** The same as in **a**, but for normalized PCs of the IOBM and NATN. In-phase (out-of-phase) are marked in red (blue). The years with both PCs exceeding 0.5 standard deviation are shown with solid dots; otherwise, shown with hollow dots

Table 1 The years of in-phase and out-of-phase of SST modes in two basins

Compound SST modes		years
NATS-IOBM	In-phase	1979, 1985, 1987, 1994, 1998, 2010, 2018
	Out-of-phase	1982, 1989, 1991, 1999, 2001, 2008, 2015
NATN-IOBM	In-phase	1982, 1984, 1987, 1991, 1994, 1996, 1999, 2000, 2003, 2010, 2013, 2017, 2018, 2019
	Out-of-phase	1979, 1983, 1985, 1988, 1998, 2004

they have different routes to influence the EPDs in the YRB, this section investigates the compound effects of the IOBM and NATS/NATN on summer EPDs in the YRB.

The representative years for the IOBM, NATS and NATN are selected based on their normalized PCs exceeding 0.5 standard deviation. On the basis of the scatterplots between the normalized PC of the Indian Ocean SST and the normalized PCs of the North Atlantic Ocean SST (Fig. 5), the years of compound IOBM and NATS modes (NATS-IOBM) and compound IOBM and NATN modes (NATN-IOBM) can be selected and divided into in-phase and out-of-phase years (Table 1).

Figure 6 shows the composite atmospheric circulation anomalies in the upper, middle and lower troposphere, and the EPDs in eastern China for NATS-IOBM and NATN-IOBM. In the anomalous fields of the compound SST modes of NATS-IOBM, significant EPD signals appear in the YRB in the in-phase composite years, whereas the out-of-phase

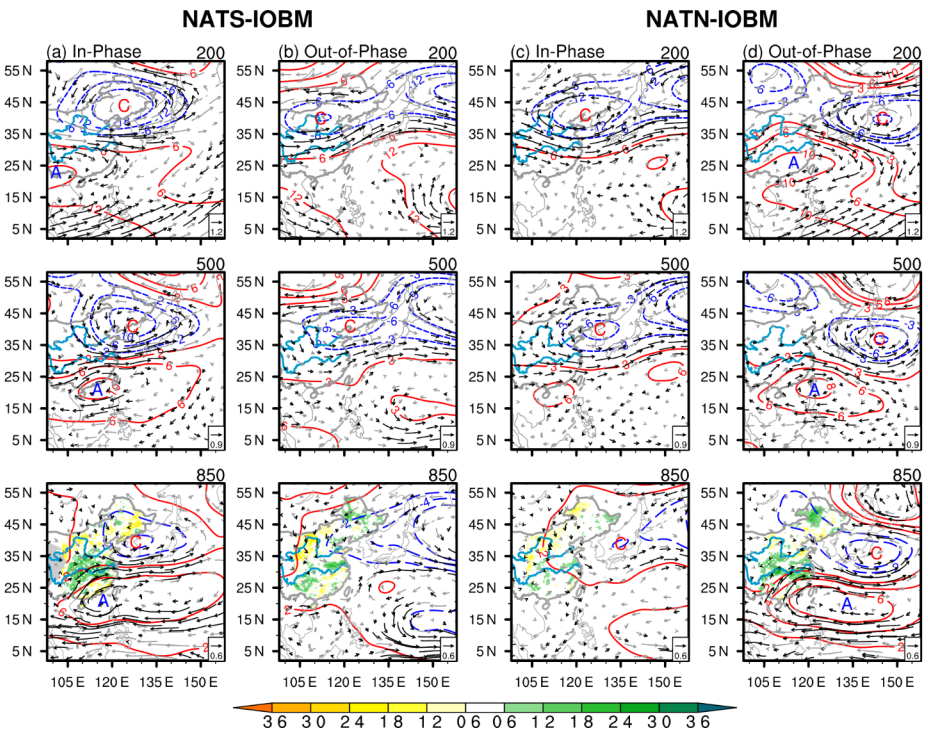

Fig. 6 The summer composite of 200 hPa, 500 hPa, and 850 hPa geopotential height (contours; unit: gpm) and wind (vectors; unit: m s^{-1}) over East Asia for the in-phase **a** and out-of-phase **b** of NATS-IOBM, and for the in-phase **c** and out-of-phase **d** of NATN-IOBM. The letters A and C indicate the centers of anticyclonic and cyclonic anomalies, respectively. The composite of wind at the 90% confidence level is shown with black arrow; otherwise, shown with grey arrows. The associated composite EPDs (shading; units: day) over eastern China is shown in the lower panels. Shading with dots is significant at the 90% confidence level

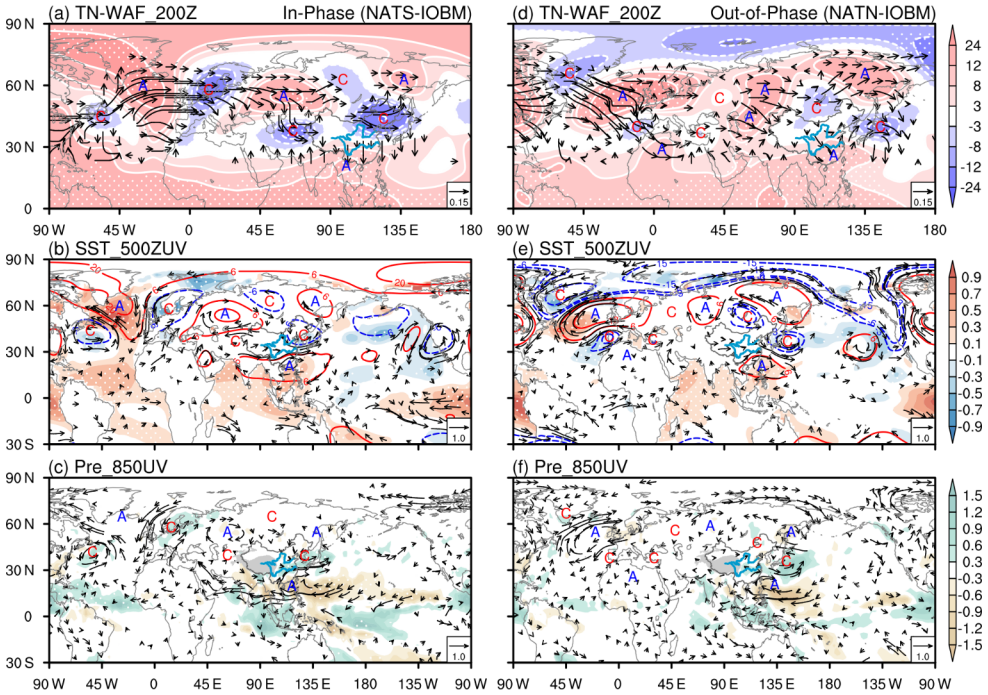

Fig. 7 The summer composite **a** 200-hPa geopotential height (shading; unit: gpm) and WAF (vectors; unit: $m^2\ s^{-2}$), **b** 500 hPa geopotential height (contours; unit: gpm), wind (vectors; unit: $m\ s^{-1}$) and SST (shading; unit: °C), and **c** 850 hPa wind (vectors; unit: $m\ s^{-1}$) and precipitation (shading; unit: $mm\ d^{-1}$) for the in-phase of NATS-IOBM. **d**–**f** The same as in **a**–**c**, but for the out-of-phase of NATN-IOBM. The composite of wind at the 90% confidence level is in black arrow. The letters A and C indicate the centers of anticyclonic and cyclonic anomalies, respectively. Shading with dots is significant at the 90% confidence level

years shows no significant EPD anomalies over eastern China (Fig. 6a and b). In contrast, in the anomalous fields of the compound SST modes of NATN-IOBM, significant EPD signals appear in the YRB in the out-of-phase years, but no EPD signals can be found in the in-phase years (Fig. 6c and d)

For the composite of the in-phase of NATS-IOBM and out-of-phase of NATN-IOBM, the PJ pattern appears over East Asia, leading to positive EPD anomalies in the YRB (Fig. 6a and d). The anomalous southwesterly wind on the northwestern flank of the WNPAC contributes to moisture transport toward the YRB, and the anomalous northwesterly wind on the southwestern flank of the NEAC inhibits the moisture going farther to the north. Thus, strong convergence of cold and warm air masses results in more EPDs in the YRB. However, it is noted that the PJ patterns in the in-phase composite of NATS-IOBM and out-of-phase composite of NATN-IOBM are distinct. The PJ pattern in the in-phase of NATS-IOBM is more westward shifted compared with that in the out-of-phase of NATN-IOBM. Because of this difference, the positive EPD anomalies in the in-phase of NATS-IOBM are much stronger and more concentrated in the YRB than that in the out-of-phase of NATN-IOBM.

To investigate the physical mechanism of the compound SST modes on the summer EPDs in the YRB, the composite dynamic and thermodynamic fields of the in-phase of NATS-IOBM and the out-of-phase of NATN-IOBM are plotted (Fig. 7). For the in-phase of NATS-IOBM, positive SSTAs over the Indian Ocean and tropical Atlantic Ocean both induce the positive precipitation anomalies in situ. The positive precipitation anomaly over the Indian Ocean induces a PJ pattern over East Asia. The precipitation-induced diabatic heating over the tropical Atlantic further stimulates the equatorial Kelvin wave response in terms of lower easterly anomalies from tropical Africa, across the northern Indian Ocean, to the western North Pacific, which in turn contribute to the strengthened WNPAC. Meanwhile, the positive precipitation anomalies over the eastern Pacific and Atlantic Ocean also lead to suppressed convection over the tropical North Pacific, which is also favorable for the WNAPC and EPDs in the YRB.

In addition to the linkages between EPDs in the YRB and the SST modes over the two basins from tropical routes, the NATS also imposes an influence on EPDs via an extratropical route. Figure 7a clearly shows that the associated atmospheric circulation anomalies are characterized by two quasi-stationary barotropic Rossby wave trains over the mid-latitude Eurasian continent. One Rossby wave train features three pairs of anomalous cyclones/anticyclones centered in the subtropical North Atlantic, west of Iceland, western Europe, Ural Mountains, North of Lake Baikal to Northeast Asia, and eastern Siberia, respectively. The other Rossby wave train shares the same first two pairs of anomalous cyclones/anticyclones with the former Rossby wave train, but bifurcates over the Ural Mountains and bends southeastward, leading to an anomalous cyclone over the Iran Plateau and an anticyclone over the Indo-China Peninsular/South China Sea. The two Rossby wave trains lead to a quasi-barotropic anomalous anticyclone over the South China Sea and an anomalous cyclone over Northeast Asia, resulting in

moisture convergence and more EPDs over the YRB. Thus, for the in-phase of IOBM and NATS, while IOBM warming and tropical warming of NATS both enhance WNPAC via tropical routes, the NATS imposes an additional anomalous NEAC through an extratropical route, leading to more pronounced positive EPD anomalies in the YRB.

For the out-of-phase of NATN-IOBM, as shown in Fig. 7d–f, IOBM warming still triggers the WNPAC in the lower troposphere via a tropical Kelvin wave response. The upper-level anomalous anticyclone over southern China and the anomalous cyclone over Japan appears at the end of the two mid-latitude Eurasian quasi-stationary Rossby wave trains, which are closely related to the NATN. One of the Rossby wave trains is characterized by four pairs of cyclone/anticyclones centered over Greenland/northeast North Atlantic, Iberian Peninsula/northern Africa, Mediterranean/central Asia, and Lake Baikal/southern China (Fig. 7d), respectively. The other Rossby wave train is located farther to the north, with seven cyclones/anticyclones centered over Greenland, northeast North Atlantic, Eastern Europe, western Siberia, Lake Baikal, eastern Siberia, and Northeast Asia, respectively (Fig. 7d). Therefore, for the out-of-phase of IOBM and NATN, while IOBM warming still exerts an influence on the WNPAC via Kelvin wave response, the negative phase of NATN influences both the SAH and the NEAC via an extratropical route, modulating the EPDs in the YRB.

In sum, the physical mechanisms of the compound SST modes of the in-phase of NATS-IOBM and the out-of-phase of NATN-IOBM on the summer EPDs in the YRB are proposed. Both the in-phase of NATS-IOBM and out-of-phase of NATN-IOBM lead to more pronounced EPDs over the YRB compared with that of the IOBM by imposing additional influences over East Asia via extratropical Rossby wave teleconnections.

5 Numerical experiments

To validate the compound impacts of the SST leading modes over the Indian Ocean and the North Atlantic Ocean on summer EPDs in the YRB, one control and four sensitivity experiments are conducted using CAM v5.3. Note that because the model has systematic bias in simulation precipitation, the EPDs derived from the model's outputs are not reliable/suitable for comparison with the observation. We calculated EPD and mean rainfall amount over the YRB and found that the EPDs are highly correlated with summer mean precipitation over YRB (figure not shown), suggesting that the mean precipitation over YRB is a good representative of EPDs in the region. Therefore, instead of EPDs, the mean precipitation response is shown in the numerical experiments.

Table 2 Design of the CAM v5.3 experiments

Experiment	The prescribed SSTA forcing
Exp_CTL	Global climatological mean SST
Exp_IOBM1	Same as Exp_CTL but adding the SSTA in the in-phase composite of NATS-IOBM in Indian Ocean (30°S-30°N, 30°E-115°E) only
Exp_IOBM + NATS	Same as Exp_CTL but adding the SSTA in the in-phase composite of NATS-IOBM in both Indian Ocean (30°S-30°N, 30°E-115°E) and North Atlantic Ocean (0°-70°N, 90°W-15°E)
Exp_IOBM2	Same as Exp_CTL but adding the SSTA in the out-of-phase composite of NATN-IOBM in Indian Ocean (30°S-30°N, 30°E-115°E) only
Exp_IOBM - NATN	Same as Exp_CTL but adding the SSTA in the out-of-phase composite of NATN-IOBM in both Indian Ocean (30°S-30°N, 30°E-115°E) and North Atlantic Ocean (0°-70°N, 90°W-15°E)

Table 2 lists the details of the five experiments. The control run (Exp_CTL) is forced by observed climatological mean (1981–2010) monthly SST. Two sets of sensitivity experiments are designed with prescribed SSTAs derived from the composites of the in-phase/out-of-phase of the IOBM and NATS/NATN modes. The first set of sensitivity experiments are run with the prescribed composite SSTAs of the positive phase of the IOBM and the positive phase of the NATS, with the first one adding composite SSTAs only in the Indian Ocean (Exp_IOBM1) and the second one adding composite SSTAs in both the Indian Ocean and the Atlantic Ocean (Exp_IOBM + NATS). The second set of sensitivity experiments are run with the prescribed composite SSTAs of the positive phase of the IOBM mode and the negative phase of the NATN, with the first one adding composite SSTAs only in the Indian Ocean (Exp_IOBM2) and the second one adding composite SSTAs in both the Indian Ocean and the Atlantic Ocean (Exp_IOBM - NATN). The composite difference between the Exp_IOBM1/Exp_IOBM2 and the Exp_CTL denotes the climate impact of the IOBM only, whereas the composite difference between the Exp_IOBM + NATS (Exp_IOBM - NATN) and the Exp_CTL denotes the compound impacts of the in-phase of NATS-IOBM (out-of-phase of NATN-IOBM).

Figure 8 shows the climate responses to the IOBM only and the in-phase of IOBM + NATS. As shown in Fig. 8a, when only positive SSTAs of the IOBM are imposed, the WNPAC appears as the response to the IOBM-induced diabatic heating, and a PJ pattern is further formed over East Asia, leading to enhanced precipitation anomalies that are similar to the observation (Fig. 2f). No remarkable Rossby wave signals can be found over the mid-latitude Eurasian continent. In contrast, when the additional SSTAs of the positive phase of NATS is imposed (Fig. 8b),

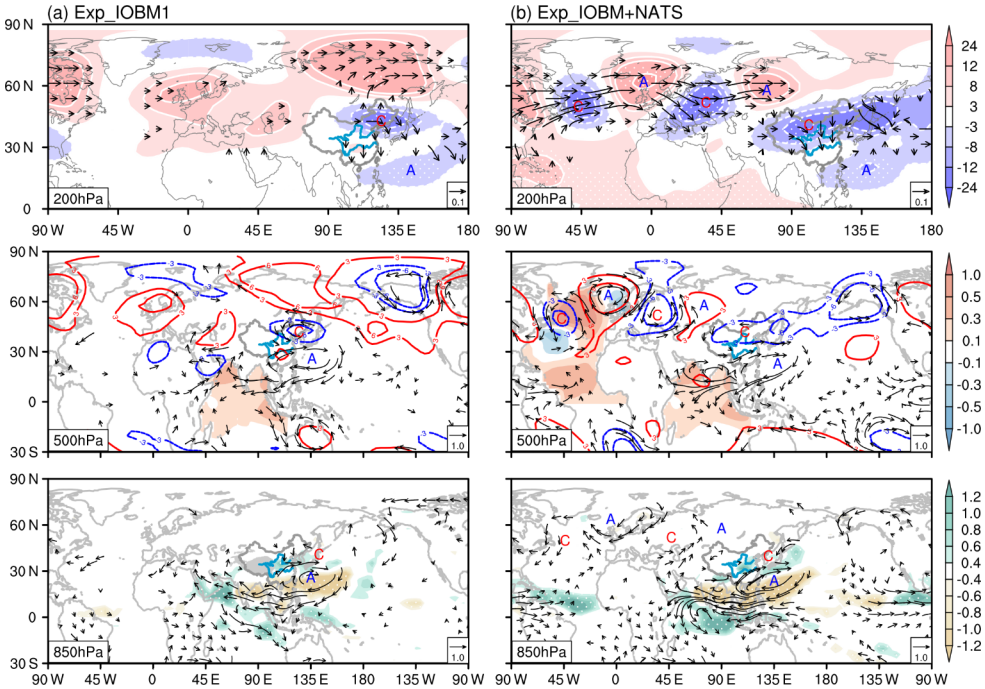

Fig. 8 **a** The composite differences between Exp_IOBM1 and Exp_CTL for 200 hPa geopotential height (shading; unit: gpm) and WAF (vectors; units: $m^2\ s^{-2}$), 500 hPa geopotential height (contours; unit: gpm), winds (vectors, unit: m s^{-1}) and SST (shading; unit: °C), and 850 hPa winds (vectors, unit: m s^{-1}) and precipitation (shading; unit: mm d^{-1}). **b** The same as in (a), but for composite differences between Exp_IOBM + NATS and Exp_CTL. The letters A and C indicate the centers of anticyclonic and cyclonic anomalies, respectively. Wind significant at 90% confidence level is in black vector, while precipitation significant at the 90% confidence level is dotted

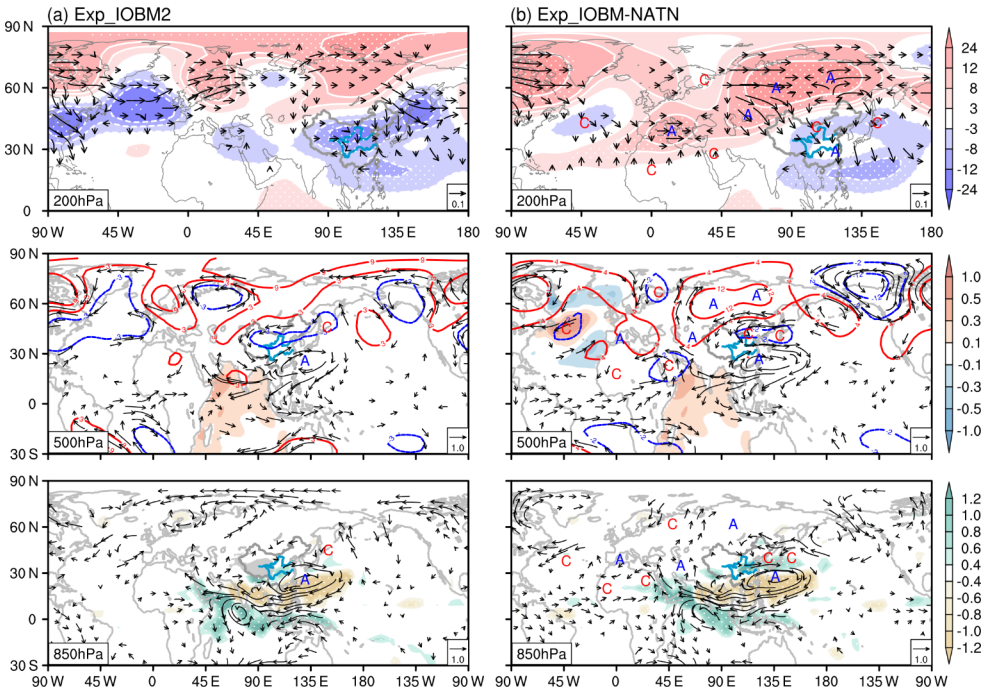

Fig. 9 The same as Fig. 8 but for the composite differences **a** between Exp_IOBM2 and Exp_CTL, and **b** between Exp_IOBM - NATN and Exp_CTL

the quasi-barotropic Rossby wave trains over mid-latitude Eurasia are reproduced with three pairs of anomalous cyclones/anticyclones centered over south of Greenland/east of Iceland, Europe/Ural Mountains, and northwestern China to Northeast Asia/South China Sea to western North Pacific, leading to stronger moisture convergence and more pronounced precipitation anomalies in the YRB. The simulated climate responses are consistent with the observations (Fig. 7a). Thus, based on numerical simulations, precipitation anomalies and EPDs in the YRB induced by IOBM warming are enhanced by the influence of the NATS via inducing the mid-latitude Rossby wave trains.

Figure 9 shows the circulation and precipitation responses to the effect of the IOBM only and to the compound effects of the IOBM and NATN. With similar IOBM warming to Fig. 8a, positive precipitation anomalies appear in the YRB with the WNPAC and NEAC (Fig. 9a) over East Asia/western Pacific sector, forming the PJ pattern. With additional

imposed SSTAs of the negative phase of NATN (Fig. 9b), the 200 hPa WAF appears, which resembles the observation with respect to the NATN (Fig. 7d). With the SSTAs of the negative phase of NATN, the northern branch of the Rossby wave train appears, with six cyclone/anticyclones centered over the northern Atlantic/Mediterranean, north of Europe/western Siberia, northern China/southern China, respectively. Compared with the impact of the IOBM only (Fig. 9a), the precipitation anomalies are much stronger and farther to the north under the additional extratropical influence of Rossby wave trains in the negative phase of NATN.

In sum, the numerical experiments generally well reproduce the observed anomalous circulation and precipitation under the single of the IOBM only, as well as the compound IOBM and North Atlantic SST modes. Both observational diagnosis and numerical simulations support that the additional influences from the positive phase of NATS and negative phase of NATN could lead to enhanced precipitation and EPDs over the YRB compared with the IOBM only by imposing an extratropical stationary Rossby wave toward East Asia.

6 Discussion and conclusion

On the basis of both observational diagnosis and numerical simulations, the compound impacts of the leading SST modes over the Indian Ocean and the North Atlantic on summer EPDs in the YRB are revealed. The first EOF mode of the Indian Ocean SST shows basin-wide uniform coherent variation (IOBM), whereas the first two EOF modes of the Atlantic Ocean SST both present a meridional tripole pattern, with one located from the tropics to extratropics (NATS) and the other located farther to the north (NATN).

The IOBM impacts the summer EPDs in the YRB by inducing a tropical Kelvin response and PJ pattern over East Asia (Fig. 10a). The NATS also independently influences the summer EPDs in the YRB. On the one hand, the tropical SST of NATS induces a Kelvin wave response to the east, leading to an enhanced WNPAC. On the other hand, an additional extratropical route of NATS impacts the EPDs in the YRB by inducing two quasi-stationary barotropic Rossby wave trains over the mid-latitudes Eurasian continent. The two Rossby wave trains lead to a quasi-barotropic anomalous anticyclone over the South China Sea and an anomalous anticyclone over Northeast Asia, resulting in moisture convergence and enhanced EPDs over the YRB. The NATN induces different Eurasian Rossby wave trains, leading to suppressed EPDs over eastern China.

For the compound impacts of the SST leading modes of the North Atlantic and the Indian Ocean, we revealed that the in-phase of NATS-IOBM and the out-of-phase NATN-IOBM exert a pronounced impact on the EPDs in the YRB. As shown in the schematic diagram (Fig. 10), the IOBM warming induces diabatic heating, which further results in a Kelvin wave response to the east. The WNPAC and PJ pattern leads to EPDs in the YRB (Fig. 10a). The in-phase of NATS imposes an additional effect on the NEAC through extratropical Rossby wave trains, and it also influences the WNPAC through a tropical Kelvin wave response and anomalous zonal circulation, leading to more pronounced positive EPD anomalies in the YRB (Fig. 10b). For the out-of-phase of NATN-IOBM, the IOBM warming influences the WNPAC via a Kelvin wave response, and the negative phase of NATN shifts the WNPAC northwestward via extratropical Rossby wave trains, leading to more northwestward-shifted EPDs in the YRB (Fig. 10c).

One may ask why the out-of-phase of NATS-IOBM and in-phase of NATN-IOBM has little influence on EPDs over the YRB. To address this question, the composite for the out-of-phase of NATS-IOBM and in-phase of NATN-IOBM are also calculated (figure not shown). It is found that both NATS in out-of-phase NATS-IOBM and NATN in in-phase of NATN-IOBM are concurrent with the positive SSTA over the central and eastern tropical Pacific. Although they could still influence East Asia circulation via extratropical routes, the impact of IOBM and convection over the Indian Ocean are largely suppressed owing to the enhanced convection over the tropical Pacific, leading to the weakened western North Pacific anomalous anticyclone and insignificant EPDs over YRB (Fig. 6b–c).

Could these SST modes in Indian Ocean and Atlantic Ocean provide useful clue for seasonal prediction of EPDs in the YRB? According to the relationship between the EPDs in the YRB and the SST modes in the two basins, the EPDs in the YRB can be reconstructed using the SSTA of the two basins based on the following equation:

$$P_{rec} = \pm\sqrt{(PC1_{IO})^2 + (PC1_{NA})^2} \times P_1 \pm \sqrt{(PC1_{IO})^2 + (PC2_{NA})^2} \times P_2$$

,where P_1 and P_2 represents the EPD pattern in the in-phase of NATS-IOBM and the out-of-phase of NATN-IOBM (Fig. 6). $PC1_{IO}$ represents the PC of the EOF mode of Indian Ocean SST, and $PC1_{NA}$ and $PC2_{NA}$ denote the first and second PC of the EOF mode of the North Atlantic SST, respectively. P_{rec} represents the reconstructed EPD pattern. The equation requires the same sign as $PC1_{IO}$.

As shown in Fig. 11, the reconstructed EPDs in the YRB are highly consistent with the observed EPDs in the region. The correlation coefficients over most of the YRB region pass the 90% confidence level. The areal mean correlation coefficient reaches 0.25 (Fig. 11a). The correlation coefficient between the observed and reconstructed year-to-year EPDs averaged over the YRB (EPDs index) is 0.52,

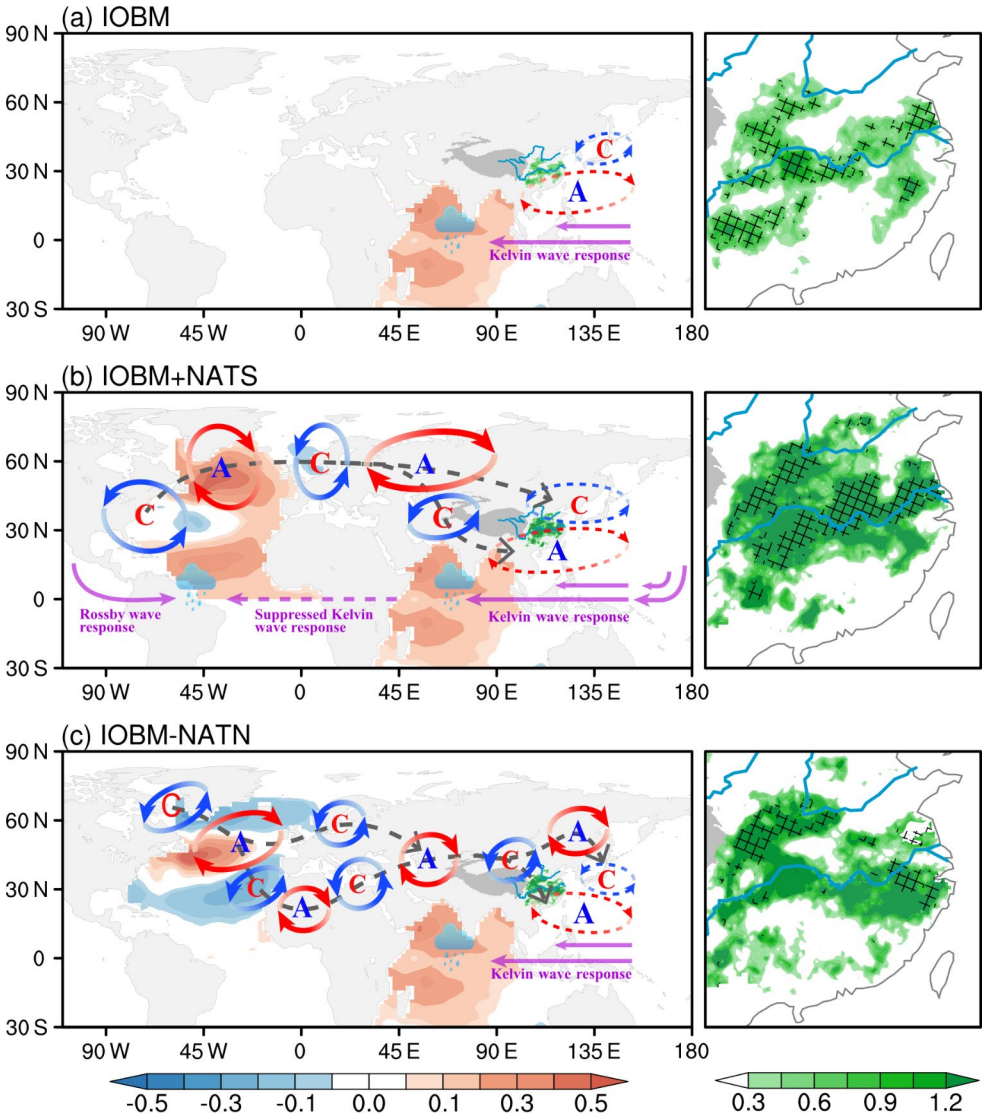

Fig. 10 Schematic diagram of the impacts of the SST modes over the Indian Ocean and the North Atlantic Ocean on the summer EPDs over the YRB. Red and blue shading delineates the SST modes. The green shading indicates the distribution of EPDs, hatching in the right panels indicates that the EPDs are significant at the 90% confidence level. The letters A and C indicate the centers of the anticyclonic and cyclonic anomalies, respectively

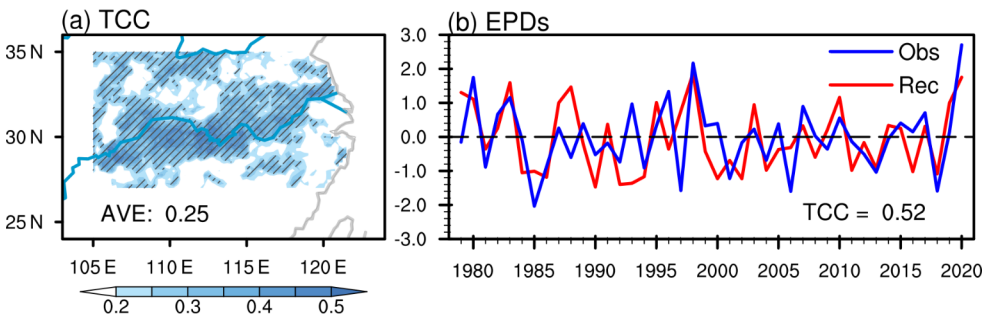

Fig. 11 **a** The distribution of the correlation coefficients (shading) between the reconstructed and observed EPDs over the YRB during 1979–2020. The hatching indicates the EPDs is significant at 90% confidence level. **b** Observed (blue) and reconstructed (red) year-to-year time series of the summer EPDs averaged over the YRB during 1979–2020

indicating that the combination of the North Atlantic and Indian Ocean SST modes can reasonably simulate the EPDs in the YRB. Given that the climate models often did well in long-lead predictions of global SST but poorly predicted the regional extreme precipitation, it is a feasible way to improve the seasonal prediction of EPDs over the YRB through a hybrid dynamical–statistical method, using statistical relationship between SST modes and EPDs in this study and the predicted SST in the state-of-the-art climate models.

Note that the correlation map between simultaneous global SST and EPDs index over YRB suggests that only

Indian Ocean and Atlantic Ocean SST are closely associated with the EPDs over YRB, no associated SST anomalies signals are found in the tropical Pacific (figure not shown). Therefore, this article only focuses on the SST modes over the Indian Ocean and Atlantic Ocean basins. However, in some cases, the diverse evolutions of the tropical central-eastern Pacific SSTA during the developing or decaying phase of ENSO may also modulate summer rainfall over YRB through atmosphere-ocean feedbacks (Pan et al. 2021; Tang et al. 2021). The compound impacts of the three basins on EPDs over YRB merits further exploration (Zheng and Wang 2021).

It is definitely true that both Atlantic and Indian Ocean SST forcing shows month-to-month (or subseasonal) variation (Wu et al. 2010; Jiang et al. 2013; Feng and Chen 2022). Whether the extratropical Rossby wave induced by the North Atlantic SST modes can be found on the subseasonal timescale and how to improve the subseasonal prediction of EPDs over the YRB remain largely unsolved.

Acknowledgements This work was supported by the National Natural Science Foundation of China (grant numbers: 42175033, 41975085 and 42088101) and the High-Performance Computing Center of Nanjing University of Information Science and Technology.

Author Contribution ZZ contributed to the study conception and design. Material preparation, data collection and analysis were performed by YF and ZZ. The first draft of the manuscript was written by ZZ, and all authors revised the manuscript.

Funding This work was supported by the National Natural Science Foundation of China (grant numbers: 42175033, 41975085 and 42088101).

Data Availability The monthly mean SST data from the improved Extended Reconstructed SST dataset V5 are available at https://psl.noaa.gov/data/gridded/data.noaa.ersst.v5.html. The monthly mean SST data from the Met Office Hadley Centre Sea Ice and SST dataset V1.1 are available at https://www.metoffice.gov.uk/hadobs/hadisst/. The monthly mean geopotential height, zonal and meridional wind provided by ERA5 are openly available at https://www.ecmwf.int/en/forecasts/datasets/reanalysis-datasets/era5. The monthly mean precipitation data provided by NOAA can be downloaded from https://psl.noaa.gov/data/gridded/data.gpcp.html.

Declarations

Ethics approval and consent to participate Not applicable.

Consent for publication Not applicable.

Competing interests The authors have no relevant financial or non-financial interests to disclose.

References

Adler RF, Sapiano MR, Huffman GJ et al (2018) The global precipitation Climatology Project (GPCP) monthly analysis (new version 2.3) and a review of 2017 global precipitation. Atmosphere 9:138. https://doi.org/10.3390/atmos9040138

Cai Y, Chen Z, Du Y (2021) The role of Indian Ocean warming on Extreme Rainfall in Central China during Early Summer 2020: without El Niño Influence. Clim Dyn 59:951–960. https://doi.org/10.21203/rs.3.rs-748847/v1

Chen J, Wang X, Zhou W et al (2018) Unusual rainfall in southern China in decaying August during extreme El Niño 2015/16: role of the western Indian Ocean and North Tropical Atlantic SST. J Clim 31:7019–7034. https://doi.org/10.1175/JCLI-D-17-0827.1

Chen W, Lee JY, Lu RY et al (2015) Intensified impact of tropical Atlantic SST on the western North Pacific summer climate under a weakened Atlantic thermohaline circulation. Clim Dyn 45:2033–2046. https://doi.org/10.1007/s00382-014-2454-4

Chen Y, Zhai P (2014) Two types of typical circulation pattern for persistent extreme precipitation in central–eastern China. Q J Roy Meteor Soc 140:1467–1478. https://doi.org/10.1002/qj.2231

Chen Z, Wen Z, Wu R et al (2016) Relative importance of tropical SST anomalies in maintaining the western North Pacific anomalous anticyclone during El Niño to La Niña transition years. Clim Dyn 46:1027–1041. https://doi.org/10.1007/s00382-015-2630-1

Chou C, Huang LF, Tu JY et al (2009) El Niño Impacts on Precipitation in the western North Pacific–East Asian Sector. J Clim 22:2039–2057. https://doi.org/10.1175/2008JCLI2649.1

Chung P, Sui C, Li T (2011) Interannual relationships between the tropical sea surface temperature and summertime subtropical anticyclone over the western North Pacific. J Geophys Res-Atmos 116:D13111. https://doi.org/10.1029/2010JD015554

Ding Y, Liu Y, Hu ZZ (2021) The record-breaking Mei-yu in 2020 and Associated Atmospheric circulation and tropical SST anomalies. Adv Atmos Sci 38:1980–1993. https://doi.org/10.1007/s00376-021-0361-2

Feng J, Chen W (2022) Respective and combined impacts of North Indian Ocean and Tropical North Atlantic SST Anomalies on the Subseasonal evolution of Anomalous Western North Pacific Anticyclones. J Clim 35:5623–5636. https://doi.org/10.1175/JCLI-D-21-0799.1

Gill AE (1980) Some simple solutions for heat-induced tropical circulation. Q J Roy Meteor Soc 106:447–462. https://doi.org/10.1002/qj.49710644905

Ham YG, Kug JS, Park JY, Jin FF (2013) Sea surface temperature in the north tropical Atlantic as a trigger for El Niño/Southern oscillation events. Nat Geosci 6:112–116. https://doi.org/10.1038/ngeo1686

He J, Wu Z, Jiang Z et al (2007) "Climate effect" of the northeast cold vortex and its influences on Meiyu. Chin Sci Bull 52:671–679. https://doi.org/10.1007/s11434-007-0053-z

He J, Zhou X, Ye R (1995) Numerical study of Ural blocking high's effect upon asian summer monsoon circulation and East China flood and drought. Adv Atmos Sci 12:361–370. https://doi.org/10.1007/BF02656985

Hersbach H, Bell B, Berrisford P et al (2020) The ERA5 global reanalysis. Q J Roy Meteor Soc 146:1999–2049. https://doi.org/10.1002/qj.3803

Hong CC, Chang TC, Hsu HH (2014) Enhanced relationship between the tropical Atlantic SST and the summertime western North Pacific subtropical high after the early 1980s. J Geophys Res-Atmos 119:3715–3722. https://doi.org/10.1002/2013JD021394

Hu Y, Deng Y, Zhou Z et al (2019) A statistical and dynamical characterization of large-scale circulation patterns associated with summer extreme precipitation over the middle reaches of

Yangtze river. Clim Dyn 52:6213–6228. https://doi.org/10.1007/s00382-018-4501-z
Huang B, Thorne PW, Banzon VF et al (2017) Extended reconstructed Sea Surface temperature, Version 5 (ERSSTv5): upgrades, validations, and Intercomparisons. J Clim 30:8179–8205. https://doi.org/10.1175/JCLI-D-16-0836.1
Huang R (2006) Progresses in Research on the formation mechanism and prediction theory of severe climatic disasters in China. Adv Earth Sci 21:564–575. https://doi.org/10.11867/j.issn.1001-8166.2006.06.0564
Jiang X, Yang S, Li J et al (2013) Variability of the Indian Ocean SST and its possible impact on summer western North Pacific anticyclone in the NCEP Climate Forecast System. Clim Dyn 41:2199–2212. https://doi.org/10.1007/s00382-013-1934-2
Jin D, Huo L (2018) Influence of tropical Atlantic sea surface temperature anomalies on the east asian summer monsoon. Q J Roy Meteor Soc 144:1490–1500. https://doi.org/10.1002/qj.3296
Klein SA, Soden BJ, Lau NC (1999) Remote Sea Surface temperature variations during ENSO: evidence for a Tropical Atmospheric Bridge. J Clim 12:917–932. https://doi.org/10.1175/1520-0442(1999)0120<917:RSSTVD>2.0.CO;2
Li CY, Mu MQ (2001) The Dipole in the equatorial Indian Ocean and its impacts on climate (in chinese). Chin J Atmos Sci 25(4):433–443. https://doi.org/10.3878/j.issn.1006-9895.2001.04.01
Li J, Ruan C (2018) The North Atlantic–Eurasian teleconnection in summer and its effects on eurasian climates. Environ Res Lett 13:024007. https://doi.org/10.1088/1748-9326/aa9d33
Li J, Zheng C, Yang Y et al (2023) Predictability of spatial distribution of pre-summer extreme precipitation days over southern China revealed by the physical-based empirical model. Clim Dyn. https://doi.org/10.1007/s00382-023-06681-2
Li T, Wang B, Wu B et al (2017) Theories on formation of an anomalous anticyclone in western North Pacific during El Niño: a review. J Meteorol Res 31:987–1006. https://doi.org/10.1007/s13351-017-7147-6
Li X, Lu R (2017) Extratropical factors affecting the variability in summer precipitation over the Yangtze River Basin, China. J Clim 30:8357–8374. https://doi.org/10.1175/JCLI-D-16-0282.1
Liu B, Zhu C, Jiang N et al (2021) Seasonal evolution of anomalous rainband over East China regulated by sea surface temperature anomalies in the Northern Hemisphere. J Clim 34(8):3087–3102. https://doi.org/10.1175/JCLI-D-20-0398.1
Liu B, Zhu C, Su J et al (2019) Record-breaking northward Shift of the western North Pacific Subtropical High in July 2018. J Meteor Soc Japan 97(4):913–925. https://doi.org/10.2151/jmsj.2019-047
Liu B, Yan Y, Zhu C et al (2020) Record-breaking Meiyu Rainfall around the Yangtze River in 2020 regulated by the Subseasonal Phase Transition of the North Atlantic Oscillation. Geophys Res Lett 47. https://doi.org/10.1029/2020GL090342. e2020GL090342
Liu Y, Ding Y (2020) Characteristics and possible causes for the Extreme Meiyu in 2020 (in chinese). Meteor Mon 46:1393–1404. https://doi.org/10.7519/j.issn.1000-0526.2020.11.001
Lorenz EN (1956) Empirical orthogonal functions and statistical weather prediction, vol 1. MIT Department of Meteorology Statistical Forecast Project Tech. Rep, p 49
Lu R, Dong B (2005) Impact of Atlantic sea surface temperature anomalies on the summer climate in the western North Pacific during 1997–1998. J Geophys Res-Atmos 110:D16102. https://doi.org/10.1029/2004JD005676
Lu R, Zhu Z, Li T et al (2021) Objective clustering of spatial patterns of summer Extreme Precipitation frequency over the Huaihe River Basin and their formation mechanisms (in chinese). Chin J Atmos Sci 45:1415–1432. https://doi.org/10.3878/j.issn.1006-9895.2105.20223
Lu T, Zhu Z, Yang Y et al (2023) Formation mechanism of the ENSO-independent summer western North Pacific anomalous anticyclone. J Clim 1–30. https://doi.org/10.1175/JCLI-D-22-0271.1
Luo JJ, Zhang RH, Behera SK et al (2010) Interaction between El Niño and Extreme Indian Ocean Dipole. J Clim 23:726–742. https://doi.org/10.1175/2009JCLI3104.1
Moberg A, Jones PD, Lister D et al (2006) Indices for daily temperature and precipitation extremes in Europe analyzed for the period 1901–2000. J Geophys Res-Atmos 111:D22106. https://doi.org/10.1029/2006JD007103
Neale RB, Gettelman A, Park S et al (2010) Description of the NCAR Community Atmosphere Model (CAM 5.0). NCAR technical note NCAR/TN-486 + STR, National Center for Atmospheric Research, Boulder
Ning L, Liu J, Wang B (2017) How does the south asian high influence extreme precipitation over eastern China? J Geophys Res-Atmos 122:4281–4298. https://doi.org/10.1002/2016JD026075
Nitta T (1987) Convective activities in the tropical western Pacific and their impact on the Northern Hemisphere summer circulation. J Meteor Soc Japan 65:373–390. https://doi.org/10.2151/jmsj1965.65.3_373
North GR, Bell TL, Cahalan RF, Moeng FJ (1982) Sampling errors in the estimation of empirical orthogonal functions. Mon Weather Rev 110:699–706. https://doi.org/10.1175/1520-0493(1982)110<0699:SEITEO>2.0.CO;2
Pan X, Li T, Sun Y, Zhu Z (2021) Cause of extreme heavy and persistent rainfall over Yangtze River in summer 2020. Adv Atmos Sci 38:1994–2009. https://doi.org/10.1007/s00376-021-0433-3
Qiao S, Chen D, Wang B et al (2021) The Longest 2020 Meiyu season over the past 60 years: Subseasonal Perspective and its predictions. Geophys Res Lett 48. https://doi.org/10.1029/2021GL093596. e2021GL093596
Qu X, Huang G (2012) Impacts of tropical Indian Ocean SST on the meridional displacement of east asian jet in boreal summer. Int J Climatol 32:2073–2080. https://doi.org/10.1002/joc.2378
Rayner NA, Parker DE, Horton EB et al (2003) Global analyses of sea surface temperature, sea ice, and night marine air temperature since the late nineteenth century. J Geophys Res-Atmos 108:4407. https://doi.org/10.1029/2002JD002670
Ren X, Yang D, Yang X (2015) Characteristics and mechanism of subseasonal eastward extension of south asian high. J Clim 28:6799–6822. https://doi.org/10.1175/JCLI-D-14-00682.1
Rong X, Zhang R, Li T (2010) Impacts of Atlantic sea surface temperature anomalies on Indo-East Asian summer monsoon-ENSO relationship. Chin Sci Bull 55:2458–2468. https://doi.org/10.1007/s11434-010-3098-3
Sun B, Li H, Zhou B (2019) Interdecadal variation of Indian Ocean basin mode and the impact on asian summer climate. Geophys Res Lett 46:12388–12397. https://doi.org/10.1029/2019GL085019
Sun S, Feng G, Zheng Z et al (2021) Study on the stable components of Atmospheric circulation during the continuous heavy rainfall of Meiyu in 2016 (in chinese). Chin J Atmos Sci 45:245–256. https://doi.org/10.3878/j.issn.1006-9895.2006.19167
Takaya K, Nakamura H (2001) A formulation of a phase-independent Wave-Activity Flux for Stationary and Migratory Quasigeostrophic Eddies on a Zonally varying Basic Flow. J Atmos Sci 58:608–627. https://doi.org/10.1175/1520-0469(2001)0580<608:AFOAPI>2.0.CO;2
Takaya Y, Ishikawa I, Kobayashi C et al (2020) Enhanced Meiyu-Baiu Rainfall in Early Summer 2020: Aftermath of the 2019 Super IOD event. Geophys Res Lett 47. https://doi.org/10.1029/2020GL090671. e2020GL090671
Tang S, Luo JJ, He J et al (2021) Toward understanding the Extreme Floods over Yangtze River Valley in June–July 2020: role of Tropical Oceans. Adv Atmos Sci 38:2023–2039. https://doi.org/10.1007/s00376-021-1036-8

Wang B, Wu R, Fu X (2000) Pacific-East Asia teleconnection: how does ENSO affect east asian climate? J Clim 13:1517–1536. https://doi.org/10.1175/1520-0442(2000)013<1517:PEATHD>2.0.CO;2

Wang B, Wu R, Li T (2003) Atmosphere–warm Ocean Interaction and its impacts on asian–australian Monsoon Variation. J Clim 16:1195–1211. https://doi.org/10.1175/1520-0442(2003)16<1195:AOIAII>2.0.CO;2

Wang B, Xiang B, Lee J-Y (2013) Subtropical high predictability establishes a promising way for monsoon and tropical storm predictions. Proc Natl Acad Sci USA 110:2718–2722. https://doi.org/10.1073/pnas.1214626110

Wu B, Li T, Zhou T (2010) Relative contributions of the Indian Ocean and local SST anomalies to the maintenance of the western North Pacific Anomalous Anticyclone during the El Niño Decaying Summer. J Clim 23:2974–2986. https://doi.org/10.1175/2010JCLI3300.1

Wu J, Gao X (2013) A gridded daily observation dataset over China region and comparison with the other datasets (in chinese). Chin J Geophys 56:1102–1111. https://doi.org/10.6038/cjg20130406

Wu Z, Li J, Jiang Z et al (2012) Possible effects of the North Atlantic Oscillation on the strengthening relationship between the east asian summer monsoon and ENSO. Int J Climatol 32:794–800. https://doi.org/10.1002/joc.2309

Xie SP, Hu K, Hafner J et al (2009) Indian Ocean Capacitor Effect on Indo–Western Pacific Climate during the summer following El Niño. J Clim 22:730–747. https://doi.org/10.1175/2008JCLI2544.1

Xie SP, Kosaka Y, Du Y et al (2016) Indo-western Pacific ocean capacitor and coherent climate anomalies in post-ENSO summer: a review. Adv Atmos Sci 33:411–432. https://doi.org/10.1007/s00376-015-5192-6

Xu S, Qi L (2022) Critical influence of the Northeast cold vortex in different positions on precipitation. Clim Dyn 1–15. https://doi.org/10.1007/s00382-022-06365-3

Yang J, Liu Q, Xie SP et al (2007) Impact of the Indian Ocean SST basin mode on the asian summer monsoon. Geophys Res Lett 34:L02708. https://doi.org/10.1029/2006GL028571

Yang Y, Zhu Z, Shen X et al (2023) The influences of Atlantic sea surface temperature anomalies on the ENSO-independent interannual variability of east asian summer monsoon rainfall. J Clim 36:677–691. https://doi.org/10.1175/JCLI-D-22-0061.1

Yuan F, Chen W, Zhou W (2012) Analysis of the role played by circulation in the persistent precipitation over South China in June 2010. Adv Atmos Sci 29:769–781. https://doi.org/10.1007/s00376-012-2018-7

Zhang MJ, Wang X, Chen LL et al (2022) Seasonal transition of precedent Indian Ocean basin mode and subsequent Indian Ocean Dipole without El Niño–Southern Oscillation impact. Int J Climatol 1–9. https://doi.org/10.1002/joc.7793

Zhang P, Wu Z, Jin R (2021) How can the winter North Atlantic Oscillation influence the early summer precipitation in Northeast Asia: effect of the Arctic sea ice. Clim Dyn 56:1989–2005. https://doi.org/10.1007/s00382-020-05570-2

Zhang Q, Zheng Y, Singh VP et al (2017a) Summer extreme precipitation in eastern China: mechanisms and impacts. J Geophys Res-Atmos 122:2766–2778. https://doi.org/10.1002/2016JD025913

Zhang R, Min Q, Su J (2017b) Impact of El Niño on atmospheric circulations over East Asia and rainfall in China: role of the anomalous western North Pacific anticyclone. Sci China Earth Sci 60:1124–1132. https://doi.org/10.1007/s11430-016-9026-x

Zheng J, Wang C (2021) Influences of three oceans on record-breaking rainfall over the Yangtze River valley in June 2020. Sci China Earth Sci 64:1607–1618. https://doi.org/10.1007/s11430-020-9758-9

Zhou ZQ, Xie SP, Zhang R (2021) Historic Yangtze flooding of 2020 tied to extreme Indian Ocean conditions. Proc Natl Acad Sci USA 118:e2022255118. https://doi.org/10.1073/pnas.2022255118

Zuo J, Li W, Sun C et al (2013) Impact of the North Atlantic sea surface temperature tripole on the east asian summer monsoon. Adv Atmos Sci 30:1173–1186. https://doi.org/10.1007/s00376-012-2125-5